Article

Cytoskeletal to Nuclear Strain Transfer Regulates YAP Signaling in Mesenchymal Stem Cells

Tristan P. Driscoll,[1,2] Brian D. Cosgrove,[1,2] Su-Jin Heo,[1,2] Zach E. Shurden,[1,2] and Robert L. Mauck[1,2,3,4,*]
[1]McKay Orthopaedic Research Laboratory, Department of Orthopaedic Surgery, Perelman School of Medicine, [2]Department of Bioengineering, School of Engineering and Applied Science, and [3]Department of Mechanical Engineering and Applied Mechanics, School of Engineering and Applied Science, University of Pennsylvania, Philadelphia, Pennsylvania; and [4]Translational Musculoskeletal Research Center, Philadelphia VA Medical Center, Philadelphia, Pennsylvania

ABSTRACT Mechanical forces transduced to cells through the extracellular matrix are critical regulators of tissue development, growth, and homeostasis, and can play important roles in directing stem cell differentiation. In addition to force-sensing mechanisms that reside at the cell surface, there is growing evidence that forces transmitted through the cytoskeleton and to the nuclear envelope are important for mechanosensing, including activation of the Yes-associated protein (YAP)/transcriptional coactivator with PDZ-binding motif (TAZ) pathway. Moreover, nuclear shape, mechanics, and deformability change with differentiation state and have been likewise implicated in force sensing and differentiation. However, the significance of force transfer to the nucleus through the mechanosensing cytoskeletal machinery in the regulation of mesenchymal stem cell mechanobiologic response remains unclear. Here we report that actomyosin-generated cytoskeletal tension regulates nuclear shape and force transmission through the cytoskeleton and demonstrate the differential short- and long-term response of mesenchymal stem cells to dynamic tensile loading based on the contractility state, the patency of the actin cytoskeleton, and the connections it makes with the nucleus. Specifically, we show that while some mechanoactive signaling pathways (e.g., ERK signaling) can be activated in the absence of nuclear strain transfer, cytoskeletal strain transfer to the nucleus is essential for activation of the YAP/TAZ pathway with stretch.

INTRODUCTION

Mesenchymal stem cells (MSCs) are a popular cell source for tissue engineering and regenerative medicine applications, given their multilineage differentiation potential. In addition to soluble factors, the differentiation of these cells can be regulated by mechanical cues from the microenvironment, including passive inputs such as substrate stiffness (1) or cell adhesion area (2) as well as active inputs such as dynamic compression (3) or tension (4). Interpretation of these mechanical cues requires cytoskeletal tension, which enables cells to probe their surroundings (1,2) and translate physical cues into changes in biologic activity. Cytoskeletal tension also regulates a number of mechanical and structural attributes of the cell, which are important for cellular interpretation of mechanical signals, and can change with differentiation status (5). Given that the downstream application of stem cells often involves their placement into a mechanically loaded microenvironment, it is critical to elucidate the relationship between physical inputs and translation of these signals to biologic activity in stem cell populations.

The attachments that cells make to molecules in their immediate microenvironment and to one another are mechanosensitive, growing or shrinking in a force-dependent manner (6). Numerous molecules located at or within the cell membrane are mechanosensitive. These include stretch-activated ion channels, which open when mechanical force is applied (7), and integrin associated molecules, such as FAK, paxillin, talin, and vinculin, all of which activate with force (8–12) by changing their conformational state under load and exposing cryptic binding sites that recruit or activate molecules involved in downstream signaling (13,14). Additionally, forces within this tensed actin cytoskeleton are transmitted to subcellular organelles, the largest and stiffest of these being the nucleus (15). Cytoskeletal forces regulate both stress and strain within the nucleus, through connections mediated by the linker of nucleoskeleton and cytoskeleton (LINC) complex. This contractile prestress in the cytoskeletal network is necessary for the rapid activation of Src kinase deep within the cell, at cytoskeletal intersection points (16). Moreover, in isolated nuclei, stretching of the actin binding LINC complex component nesprin 1 induces a rapid Src kinase-dependent phosphorylation of emerin on the inner nuclear membrane (17). This phosphorylation event changes association with the nuclear structural protein lamin A, resulting in stiffening of the nucleus and regulation of downstream transcription of mechanically regulated genes. Thus, transfer of mechanical force through the tensed actin cytoskeleton to the nucleus is likely important in mechanosensing, and identifying specific pathways

Submitted November 17, 2014, and accepted for publication May 12, 2015.
*Correspondence: lemauck@mail.med.upenn.edu
Editor: David Odde.

0006-3495/15/06/2783/11 $2.00
http://dx.doi.org/10.1016/j.bpj.2015.05.010

that are regulated by this strain transfer mechanism is therefore an important goal.

One pathway that mediates MSC mechanosensing is the Yes-associated protein (YAP)/transcriptional coactivator with PDZ-binding motif (TAZ) mechanotransduction pathway (18). YAP relays mechanical input through a Rho-GTPase-dependent translocation to the nucleus, where it acts to regulate gene transcription (18). These mechanotransductive elements are likewise required for substrate-stiffness-induced differentiation of MSCs. Additionally, it has been shown that the YAP/TAZ pathway can be activated with dynamic tensile loading of myoblasts (19), and that mutations in the nuclear lamina or in components of the LINC complex perturb this response (17,19). Therefore, mechanosensing through YAP may depend on forces transmitted through the cytoskeleton and to the nucleus.

Both matrix organization and composition play a role in determining how strain is transmitted through the cell and to the nucleus. In native tissues, nuclear strain transmission is variable, depending on tissue type and local matrix properties (20–22). In three-dimensional aligned fibrous environments, nuclear strain transfer depends on a patent actin cytoskeleton, but is independent of microtubules and intermediate filaments (23). Furthermore, biologic response in this context depends on the direction of stretch with respect to fiber orientation (24), and cell realignment does not occur with long-term stretch (4) as it does on two-dimensional surfaces. The organization of the microenvironment in which a cell resides thus plays a critical role in mediating both the transfer of strain through the cell and the response of that cell to loading.

Despite a growing understanding that mechanosensing occurs at the nuclear membrane (in addition to traditional focal adhesions at the cell periphery), the exact role that transfer of strain to the nucleus plays in the response of MSCs to tensile stretch is not clear, and the importance of nuclear strain versus nuclear stress concentrations is as yet unknown. Further, there likely exist mechanosensitive pathways that depend specifically on nuclear strain transfer and nuclear deformation, as well as others that signal primarily from cell-membrane-associated mechanosensitive signaling modules. In this study, we assayed the extent to which nuclear and cytoskeletal prestress and nuclear connectivity regulate transmission of strain to the MSC nucleus, and the role of this prestress in the regulation of both short- and long-term interpretation of mechanical cues. We employed both static and dynamic tensile stretch, in the presence or absence of pharmacologic regulators of cytoskeletal tension and filamentous actin patency, and with molecular modulation of cytoskeletal-to-nuclear connectivity, to determine the roles that cytoskeletal tension and nuclear deformation play in activating the early response (ERK1/2 MAP kinase, YAP/TAZ) and longer-term transcriptional programs in response to dynamic mechanical cues.

MATERIALS AND METHODS

Scaffold fabrication

Aligned electrospun scaffolds were generated as described in Nerurkar et al. (25) by electrospinning a 14.3% w/v solution of poly(ε-caprolactone) (Bright China, Hong Kong, China) in 1:1 mixture of *n*,*n*-dimethylformamide and tetrahydrofuran (Fisher Chemical, Fairlawn, NJ). This solution was extruded at a rate of 2.5 mL/h through a spinneret (18 gauge stainless-steel needle) charged to +13 kV. Alignment was instilled by collecting fibers onto a grounded mandrel rotating with a surface velocity of ~10 m/s. Scaffold mats (~1-mm thick) were removed from the mandrel and cut into 65 × 5 mm segments with the long axis oriented in the prevailing fiber direction. Scaffold segments were disinfected and rehydrated in decreasing concentrations of ethanol (100, 70, 50, and 30%; 1 h/step) and rinsed twice in PBS (phosphate-buffered saline). Before cell seeding, scaffolds were coated in fibronectin (Sigma-Aldrich, St. Louis, MO) for 12–18 h, 20 μg/mL in PBS.

Cell isolation and seeding

MSCs derived from bovine bone marrow were isolated from the tibiofemoral trabecular bone marrow of juvenile calves and plated onto 15-cm tissue culture dishes (26). MSCs were expanded in basal media (high glucose DMEM with 10% FBS and 1% PSF) for two passages before seeding. For monolayer experiments, MSCs were seeded onto glass slides or fibronectin-coated poly-acrylamide gels and cultured overnight in serum-free, chemically defined media (high glucose DMEM with 1× PSF, 0.1 μM dexamethasone, 50 μg/mL ascorbate 2-phosphate, 40 μg/mL L-proline, 100 μg/mL sodium pyruvate, 6.25 μg/mL insulin, 6.25 μg/mL transferrin, 6.25 μg/mL selenous acid, 1.25 mg/mL bovine serum albumin, and 5.35 μg/mL linoleic acid) (27). For stretch studies, cells were seeded onto 65 × 5 mm fibronectin-coated aligned electrospun scaffolds at a density of 2×10^5 cells per side (protein and mRNA studies) or 5×10^4 cells per side (image-based studies).

Pharmacologic regulation of contractility

Contractility was altered via the application of various pharmacologic agents. Contractility was decreased using the myosin inhibitor Blebbistatin (Sigma-Aldrich), the myosin light chain kinase (MLCK) inhibitor ML7 (Tocris Biosciences, Bristol, UK), the ROCK inhibitor Y27632 (Calbiochem Merck, Darmstadt, Germany), and the actin polymerization inhibitor cytochalasin D (Sigma-Aldrich). The ROCK agonist LPA (lysophosphatidic acid) (Sigma-Aldrich) was used to transiently increase contractility. For experiments focused on dose dependence, concentration was varied across a range previously reported in the literature. For all other experiments, contractility modulators were set at defined levels: Bleb (Blebbistatin) 50 μM, ML7 25 μM, Y27632 10 μM; CytoD (Cytochalasin D) 2.5 μM; and LPA 50 μM. All inhibitors were added 1 h before fixing or stretching, while activators (LPA) were added 15 min before fixing or stretching.

Immunofluorescence

Cells seeded on glass slides overnight were fixed with 4% paraformaldehyde for 20 min at 37°C, then washed and permeabilized with 0.05% Triton X-100 in PBS supplemented with 320 mM sucrose and 6 mM magnesium chloride. Cells were incubated with anti-YAP antibody in 1% BSA in PBS (No. sc-101199, 1:200; Santa Cruz Biotechnology, Dallas, TX) overnight at 4°C, washed three times with PBS, and then incubated for 60 min at room temperature with Alexa-Fluor 488 or 546 phalloidin (1:1000; Molecular Probes, Eugene, OR) and Alexa-Fluor 546 or 488 goat anti-mouse secondary (1:200; Molecular Probes). Cells were washed three times and mounted with DAPI-containing mounting medium (ProLong Gold Antifade

Reagent; Molecular Probes). Images were taken using an Eclipse TE2000-U inverted epi-fluorescence microscope with 20× objective (Nikon, Melville, NY) and quantified using a custom MATLAB program (The MathWorks, Natick, MA). DAPI images were edge-detected using the Canny edge-detection algorithm, and the nuclear area was quantified. The nuclear outline was then used as a mask to quantify F-actin staining intensity in the vicinity of the nucleus. For YAP/TAZ staining on glass, average staining intensity in the nucleus and within the cytoplasm was quantified using the software ImageJ (National Institutes of Health, Bethesda, MD); these intensities were used to calculate a nuclear/cytoplasmic YAP. Nuclear height was measured using ImageJ, based on DAPI staining from orthogonal *Y-Z* images generated from confocal *z*-stacks (model No. LSM 510 with 60× oil objective, acquired with z-resolution of 0.37 μm/pixel; Carl Zeiss, Oberkochen, Germany).

Traction force microscopy

Polyacrylamide (PA) hydrogels (Young's modulus, $E = 5$ kPa) were prepared as in Aratyn-Schaus et al. (28). A quantity of 0.2-μm-diameter fluorescent microspheres (No. F8810; Invitrogen, Carlsbad, CA) was mixed into PA at 1% v/v before polymerization. Fibronectin (20 μg/mL) coating of gel surfaces was accomplished with 2 mg/mL sulfo-SANPAH (No. 22589; Pierce Protein Biology/Life Technologies, Rockford, IL). Small drops of a UV-curable fixative (NOA68; Norland Products, Cranbury, NJ), were used to secure the slides in a live cell imaging chamber. Gels were subsequently washed three times with PBS and sterilized under germicidal UV light for 1 h. In all traction force experiments, MSCs were seeded at a density of 3000 cells/cm^2 and allowed to attach for 20 h before traction force microscopy was performed. Phase contrast and fluorescent images of multiple cells and embedded beads were captured at 40× magnification on a DeltaVision Deconvolution Microscope (GE Healthcare Life Sciences, Marlborough, MA). Image sequences for each cell were taken at three points: 1) before addition of contractility altering-agents, 2) after specified incubation times in the presence of these agents, and 3) after cell lysis with SDS (sodium dodecyl sulfate) buffer. All imaging was performed in an environmental chamber (37°C, 5% CO_2). Traction force microscopy data analysis (stack alignment, particle image velocimetry, and Fourier transform traction cytometry) was performed using a freely available plugin suite for ImageJ, created by Tseng et al. (29), which was adapted from Dembo and Wang (30). For Fourier transform traction cytometry, the Poisson's ratio of the PA gel was assumed to be 0.45 and a regularization parameter of $2e-9$ was used. Using a custom MATLAB script, traction force vector maps were analyzed to determine average traction stress generated by each cell and total force exerted per cell. Cell area was determined from the corresponding phase contrast images in ImageJ.

Static tensile stretch and analysis of nuclear deformation

Cells seeded on aligned scaffolds were stained with Hoechst (5 μg/mL, Molecular Probes) in high-glucose phenol-free DMEM containing HEPES for 10 min at 37°C. Static stretch was applied to determine the role of cytoskeletal tension in nuclear deformation. Scaffolds ($n > 4$ per group) were stretched up to 15% strain in 3% increments using a tensile device mounted on an Eclipse TE2000-U inverted epi-fluorescence microscope (Nikon) using a 20× Plan Fluor ELWD objective with a tunable correction collar. Nuclear deformation at each step was quantified ($n > 50$ cells per group) using a custom MATLAB program by calculating the ratio of nuclear principal lengths normalized to 0% strain. A Canny edge-detection algorithm was used to detect outer nuclear edges based on gradients in signal intensity. Edges were then dilated, filled, and grouped into clusters. Principal component analysis was performed on the clusters to identify principal lengths of the nucleus as in Nathan et al. (23). A nuclear deformation index (*NDI*) was then calculated for each experimental group by normalizing nuclear deformation at each strain level to the mean deformation observed for the control group at that same strain level. To calculate this index, the average nuclear deformation (nuclear aspect ratio normalized to undeformed state (*nNAR*)) was calculated at each strain level. These averages were used to normalize the nuclear deformation at each of the five strain levels ($i = 1$–5) to the associated deformation in the control group at that strain level using the formula

$$NDI = \frac{(nNAR_{Ti} - 1) - (nNAR_{Ci\mathrm{Ave}} - 1)}{(nNAR_{C15\%\mathrm{Ave}} - 1)} \times 100,$$

where i indicates the applied strain level (3, 6, 9, 12, 15%), T indicates treatment group, C indicates control group, and *Ave* indicates average at that strain level.

Local Lagrangian strains were also calculated using triads of nuclei as fiducial markers at each strain level to ensure consistent local deformations across scaffolds and experimental conditions. To begin, the displacements for each point were calculated based on a reference image. These displacements were then used to calculate the deformation gradient tensor $\mathbf{F}$,

$$\mathbf{F}_{ij} = \mathbf{dx}_i / \mathbf{dX}_j,$$

where x indicates the deformed point locations, X indicates the undeformed locations, and i and j indicate the principal directions. This tensor can then be used to calculate the Lagrangian strain tensor $\mathbf{E}$:

$$\mathbf{E}_{ij} = \frac{1}{2}\left(\mathbf{F}^{\mathbf{T}}\mathbf{F} - \mathbf{I}\right).$$

Components of this tensor give the two-dimensional strains in the two principal directions as well as the shear strain.

Dynamic tensile stretch

Dynamic stretch (3% strain, 1Hz) was applied in a CO_2 incubator using a custom bioreactor system (8). For analysis of pERK1/2 response, stretch was applied for 15 min with inhibitors (Bleb 50 μM, ML7 25 μM, Y27632 10 μM) added 1 h before stretch and LPA (50 μM) added 15 min before stretch. For quantification of nuclear YAP with stretch, cells were loaded for 30 or 360 min and fixed and stained with anti-YAP antibody, phalloidin, and DAPI immediately or 12 h after cessation of loading, with inhibitors added 1 h before stretch. For YAP analysis on scaffold, cells were imaged using an A1 laser-scanning confocal microscope with 20× objective (Nikon). *Z*-stacks were acquired at 0.75-μm slice thickness over the entire cell with the slice centered at the nucleus used for quantification of the nuclear/cytoplasmic YAP. For analysis of the gene expression, stretch was applied on two consecutive days for 6 h per day with inhibitors added 1 h before stretch on each day of loading.

Western blotting

Cells were seeded on aligned scaffolds for 2 days, dynamically loaded for 15 min at 1 Hz to 3% strain, washed once with PBS, and lysed in RIPA buffer (50 mM Tris-HCl pH 8.0, 150 mM sodium chloride, 1.0% Triton X-100, 0.1% SDS, with 1% protease inhibitor cocktail and 1% phosphatase inhibitor cocktail, both from Sigma-Aldrich) to isolate total cellular proteins. Protein isolates were cleared of insoluble cellular debris by centrifugation (15,000 × g for 15 min) and protein concentration was quantified using the Lowry assay (Bio-Rad, Hercules, CA). Samples were denatured by boiling for 5 min in reducing buffer containing 2% β-mercaptoethanol. Proteins were separated on 4–15% gradient SDS polyacrylamide gels and transferred to nitrocellulose membranes. Membranes were blocked with 5% BSA (bovine serum albumin) in Tris-buffered saline containing 0.1% TSB-T (TWEEN 20) and probed with p44/p42 MAPK (ERK1/2)

or phospho-p44/p42 MAPK (pERK1/2) (Cell Signaling, Danvers, MA). Membranes were washed three times with TBS-T and treated with anti-rabbit peroxidase conjugated secondary antibody in 5% BSA-TBS-T (1:1000; Cell Signaling). Blots were developed using SuperSignal West Pico Chemiluminescent Reagent (Pierce Protein Biology/Life Technologies) and exposed to CL-Exposure film (Thermo Fisher Scientific, Waltham, MA).

Quantitative real-time polymerase chain reaction

Changes in gene expression were determined by real-time (RT) polymerase chain reaction (PCR). MSCs were seeded on aligned nanofibrous scaffolds for two days in chemically defined media and then loaded into the custom tensile bioreactor with or without pharmacologic regulators of contractility (Bleb 50 μM, ML7 25 μM, and Y27632 10 μM) for 1 h before loading on each day of loading. Cells were dynamically stretched to 3% strain at 1Hz for 6 h on two consecutive days. After the second loading, samples were snap-frozen in Trizol, and mRNA was subsequently isolated by phenol-chloroform extraction. RNA concentration was quantified (ND-1000; Nanodrop Technologies, Wilmington, DE) and cDNA synthesized using the SuperScript II First Strand Synthesis kit (Invitrogen, Carlsbad, CA). PCR was performed with gene-specific primers using a StepOnePlus RT PCR machine and the Fast SYBR Green reaction mix (Applied Biosystems, Foster City, CA).

Expression levels of aggrecan (AGG) (CCTGAACGACAAGACCAT CGA and TGGCAAAGAAGTTGTCAGGCT), connective tissue growth factor (CTGF) (CGTGTGCACCGCTAAAGATG and GGAAAGAC TCTCCGCTCTGG), and scleraxis (SCX) (GAACACCCAGCCCAAACA GAT and TCCTTGCTCAACTTTCTCTGGTT) were determined and normalized to the housekeeping gene glyceraldehyde-3-phosphate dehydrogenase (GAPDH) (ATCAAGAAGGTGGTGAAGCAGG and TGAG TGTCGCTGTTGAAGTCG).

Lentiviral delivery of miRNA

Knockdown of nesprin-1 giant was accomplished using inhibitory microRNA delivered via a lentiviral vector-based system (Block-it Lentiviral Pol II miR RNA_i Expression System with EmGFP; Invitrogen). Three nesprin-1 giant vectors (targeted to the N-terminal actin binding calponin homology domain) were designed based on the bovine sequence for nesprin-1 giant and the miRNA sequence (TGCCGAGGACCTTCATC TTCT), which resulted in the highest levels of knockdown, was used for subsequent studies. The miRNA-sequence-containing oligos were annealed and ligated into pCDNA6.2-GW/Em-GFP. The miRNA-containing cassettes were then transferred to pLenti6/V5-DEST via the Gateway cloning reaction and sequenced before viral production in HEK293FT cells. Virus (media supernatant) was titered by infection of MSCs and selection for blasticidin resistance (at 14 days) or analysis of %GFP positive cells (at 4 days) by flow cytometry (using the FACSCaliber with CELLQUEST PRO software by Becton Dickinson, Franklin Lakes, NJ). For all experiments, cells were infected with virus overnight. Four days postinfection, cells were trypsinized and reseeded onto glass, polyacrylamide gels, tissue culture plastic, or aligned electrospun scaffolds. Knockdown was verified by dot blot for nesprin 1 after 1-MDa size filtration.

Statistical analysis

All experiments were performed for 2–3 MSC donors and scaffold batches per condition. Statistical comparisons were performed using one- or two-way analysis of variance (ANOVA) with Tukey's post hoc testing used to make pairwise comparisons between groups. Statistical significance was set at $p < 0.05$. For nuclear deformation experiments, single cells were tracked and comparisons made using two-way repeated measures ANOVA with Tukey's post hoc testing.

RESULTS

Contractility regulates basal nuclear shape

Acto-myosin-based contractility has previously been shown to play an important role in regulating nuclear shape and organization in a variety of cell types (31–33). To determine the extent to which actin and intracellular tension regulate nuclear shape (aspect ratio, height, and projected area) in MSCs, cells were treated with varying levels of pharmacologic regulators of actin assembly and contractility. Subsequently, treated MSCs were stained with phalloidin and DAPI to visualize the actin cytoskeleton and nuclei, respectively. Decreasing contractility by inhibition of either ROCK (Y27632) or actin polymerization (CytoD) resulted in a dose-dependent loss of stress fibers (Fig. 1 *A*) as well as a dose-dependent decrease in the projected area of the nucleus (Fig. 1 *B*). Decreasing contractility by inhibition of myosin (Bleb) or MLCK (ML7) activity did not significantly alter F-actin structure, although it still resulted in a dose-dependent decrease in nuclear projected area (Fig. 1, *A* and *B*). Activation of contractility using the ROCK agonist LPA increased stress fiber density, but did not significantly alter the nuclear projected area (Fig. 1, *A* and *B*). To quantify the extent to which these regulators of contractility altered the number of stress fibers passing over and under the nucleus, the nuclear outline was used as a mask to crop actin images, and the average intensity of filamentous actin in this nuclear region was quantified (Fig. 1 *C*). Consistent with previous observations, inhibition of ROCK or actin polymerization caused a significant loss of stress fibers in the vicinity of the nucleus while inhibition of MLCK increased the average intensity (due to similar actin signal coupled with a decrease in the projected nuclear area) (Fig. 1 *D*). Treatment with the ROCK agonist LPA significantly increased actin intensity over the nucleus. These alterations in contractility did not significantly affect the aspect ratio of the nucleus, indicating equal shortening of both nuclear axes with inhibition (not shown). To assess the extent to which these alterations perturbed the nuclear shape in the third dimension, confocal imaging was performed and orthogonal *X-Z* slices were used to determine changes in nuclear height (Fig. 1 *E*). With inhibition of contractility (via any of the inhibitors), a significant increase in the nuclear height (~25–35%) was observed, while activation of contractility (LPA) resulted in a significant decrease in nuclear height (~20%) (Fig. 1 *F*).

Next, we sought to determine the percent change in acto-myosin contractility associated with these changes in projected nuclear area and height. Traction forces were measured using 5-kPa polyacrylamide gels that were coated with fibronectin and contained fluorescent microspheres for tracking substrate deformation. Traction force maps for single cells before and after treatment with pharmacologic agents showed substantial decreases in traction force with inhibition of ROCK or MLCK and increases in traction

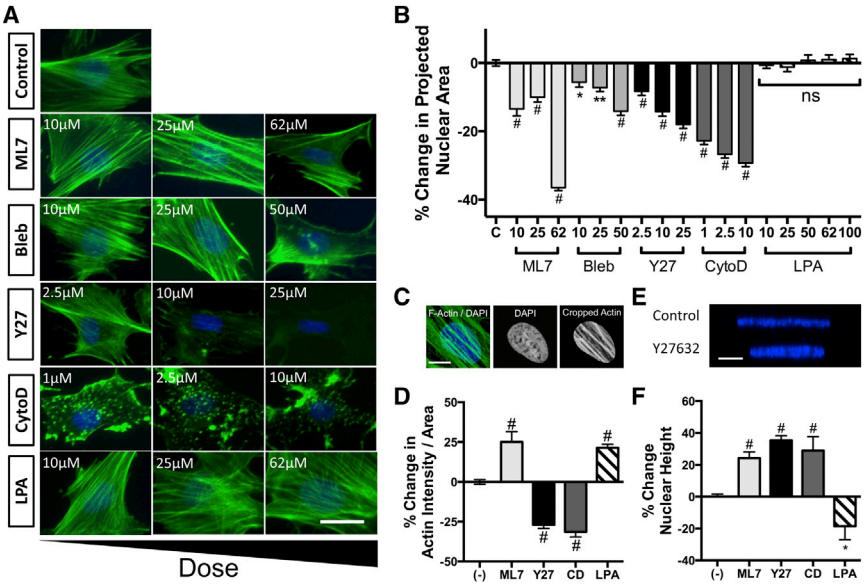

FIGURE 1 Cytoskeletal tension regulates nuclear and cytoskeletal morphology. (*A*) F-Actin (*green*) and DAPI (*blue*) images of cells seeded on glass and treated with different doses of ML7, Bleb, Y27632 (Y27), CytoD, or LPA (scale = 25 μm). (*B*) Quantification of projected nuclear area on glass (mean ± SE, $n > 85$ cells/group). (*C*) Example of F-actin in the projected area of the nucleus (scale = 10 μm), and (*D*) with quantification (mean ± SE, $n > 85$ cells/group; ML7 = 25 μM, Y27632 = 10 μM, CytoD = 10 μM, LPA = 50 μM). (*E*) Example *X-Z* slices of nuclei (scale = 5 μm) used for quantification of nuclear height (*F*). (Mean ± SE, $n > 13$ cells/group; $*p < 0.05$, $**p < 0.01$, $\#p < 0.001$ versus control; one-way ANOVA with Tukey's post hoc testing.) To see this figure in color, go online.

force with activation of ROCK (Fig. 2 *A*). Inhibition of ROCK (Y27632, 10 μM) or MLCK (ML7, 25 μM) decreased total force per cell by 80–90% while treatment with the ROCK agonist LPA (50 μM) increased total force per cell by ~60% (Fig. 2 *B*). Consistent with previous studies (18), inhibition of contractility with either Y27632 or ML7 resulted in a significant decrease in YAP localization to the nucleus (Fig. 2, *C* and *D*) when MSCs were plated on stiff (glass) substrates. Interestingly, increasing contractility via addition of LPA did not alter YAP localization in this context (suggesting that YAP nuclear localization had already reached its maximum level).

Contractility regulates transfer of strain to the nucleus

Next, we sought to determine the role that filamentous actin and intracellular tension play in the transfer of strain to the nucleus when exogenous stretch was applied to cells cultured on aligned nanofibrous scaffolds. For this, we developed a stepper-motor-driven microtensile device that allows for simultaneous tensile stretch and imaging of cells and nuclei (Fig. 3 *A*). With this system, scaffold Lagrangian strains can be quantified using triads of nuclei as fiducial markers (Fig. 3 *B*). Quantification showed that microscale strains in the stretch direction (X_1, E_{11}) were very close to the applied strain and that low shear strains (E_{12}) were observed for all groups (Fig. 3 *C*). Large lateral compressive strains (E_{22}) were observed for all groups due to the highly aligned and porous nature of the electrospun scaffolds. These scaffolds typically display a Poisson's ratio of 1.25–1.5, due to their high level of structural anisotropy.

Consistent with our previous studies (23,24), quantification of nuclear aspect ratio (NAR) with applied stretch in control MSCs showed a strain-dependent increase in NAR, with a wide distribution across the population

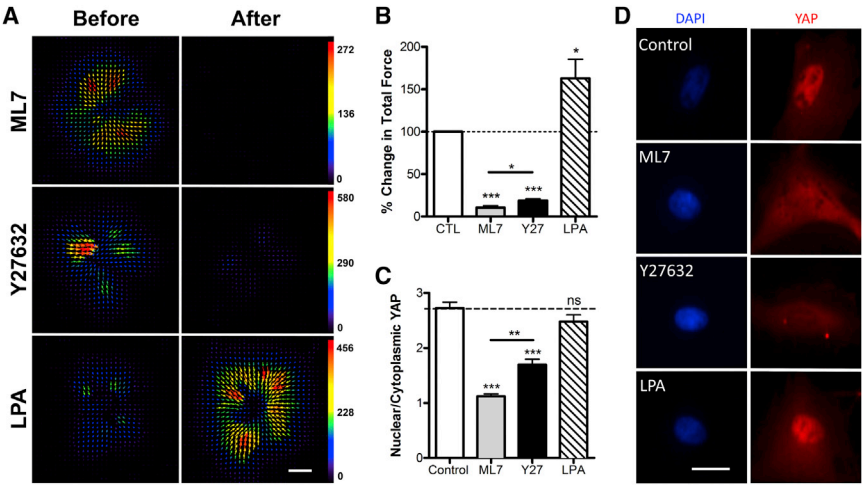

FIGURE 2 Traction force and YAP localization are regulated by ROCK and MLCK. (*A*) Traction stress maps for MSCs on 5-kPa polyacrylamide gels before and after addition of ML7, Y27632, or LPA (scale bar = 25 μm, units = Pa), (*B*) with quantification of % change in total force per cell (n = 14–20 cells per group, $*p < 0.05$, $***p < 0.001$, one-way ANOVA with Tukey's post hoc testing). Quantification of the nuclear/cytoplasmic YAP signal intensity for (*C*) MSCs seeded on glass and treated with ML7 (25 μM), Y27632 (10 μM), or LPA (50 μM), and (*D*) with example epi-fluorescent images of YAP (*red*) and DAPI (*blue*) staining (scale bar = 25 μm). To see this figure in color, go online.

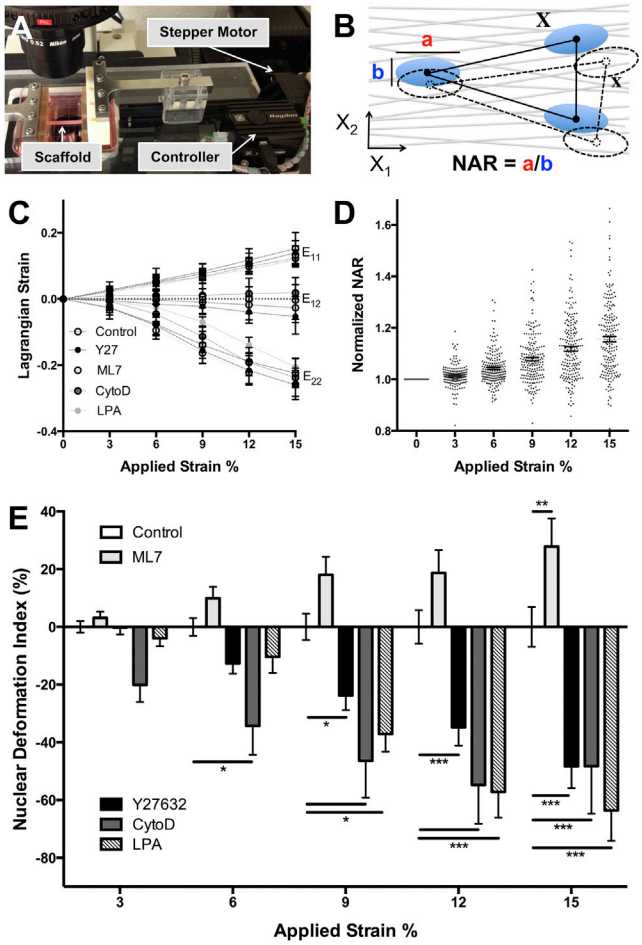

FIGURE 3 Contractility and nuclear prestrain regulate strain transmission to the nucleus. (*A*) Microtensile device used for stretch with simultaneous epi-fluorescent imaging of cell and nuclear deformation on scaffolds. (*B*) Schematic of deformation analysis indicating the nuclear aspect ratio (*NAR*) and the locations of nuclear triads in the deformed (*x*) and undeformed (*X*) states that were used for Lagrangian strain calculation. (*C*) Lagrangian strains including shear strain (E_{12}), strain in the stretch direction (E_{11}), and strain perpendicular to the stretch direction (E_{22}). (*D*) Nuclear aspect ratio (NAR) for control cells normalized to the unstrained (0% strain) case. (*E*) Nuclear deformation index (NDI, which is *NAR* normalized to untreated control cells at the same strain, *nNAR*) for cells treated with ML7 (25 μM), Y27632 (10 μM), CytoD (2.5 μM), or LPA (50 μM). Nuclei that deform more than control have a positive NDI, and nuclei that deform less than control have a negative NDI. (Mean $\pm$ SE, $n > 50$ cells/group; two-way repeated measures ANOVA with Tukey's post hoc testing.) To see this figure in color, go online.

(Fig. 3 *D*). With inhibition of ROCK or actin polymerization (with Y27632 or CytoD), a significant decrease in nuclear deformation was observed, such that nuclei deformed ~50% less than control cells (Fig. 3 *E*). Conversely, decreasing contractility by inhibition of MLCK with ML7 resulted in a significant increase in nuclear deformation (Fig. 3 *E*), potentially due to decreased nuclear prestress despite maintenance of cytoskeleton-to-nucleus connectivity. Similar results were observed for inhibition of myosin using Bleb (Fig. S1 in the Supporting Material), although in this case quantification was difficult due to the autofluorescent nature of this chemical in conjunction with the PCL scaffolds. When the baseline contractility was increased before stretch (using LPA), a significant decrease in nuclear deformation was again observed, potentially due to stabilization of the nucleus with increased actin and nuclear prestress. These results indicate that an intact actin stress fiber network and the tension in that network (exerting prestress on the nucleus) both play important roles in the conversion of extracellular strain to nuclear deformation.

Contractility regulates response to dynamic tensile stretch

Next, we sought to determine the importance of contractility and nuclear deformation in MSC response to dynamic tensile stretch. For these experiments, cells were seeded onto aligned scaffolds for two days and then dynamically stretched at 1 Hz to 3% strain for either 15 min (to assess activation of ERK1/2 signaling) or for 6 h on two consecutive days (to assess changes in gene expression). Western blots showed a significant increase in pERK1/2 with dynamic loading (DL, Fig. 4 *A*). In the presence of inhibitors of contractility, the response of pERK1/2 to loading was not prevented (Fig. 4, *A* and *B*), but did show a slightly lower fold increase with loading. This was due in part to an increase in baseline pERK1/2 with inhibition of contractility. With activation of contractility (via the addition of LPA), a significant increase in baseline pERK1/2 was observed in free swelling conditions (Fig. 4, *A* and *B*). When stretch was applied in this context, ERK1/2 showed no further increase in activation (Fig. 4 *C*). These results indicate that cytoskeletal tension is not essential for the activation of ERK1/2 with tensile stretch, but that increases in cytoskeletal tension can activate ERK1/2.

When dynamic loading was extended over a longer period of time (two days for 6 h per day), untreated MSCs showed a significant increase in expression of the cartilage marker aggrecan, the growth factor CTGF, and the tendon transcription factor scleraxis. Inhibition of contractility with Bleb, Y27632, or ML7 abrogated the stretch-induced expression of CTGF (Fig. 4 *E*) and scleraxis (Fig. 4 *F*). However, stretch-induced upregulation of aggrecan expression was only partially inhibited when contractility was reduced, and this depended on the specific contractility inhibitor employed. With inhibition of contractility using ML7 or Y27632, a substantial reduction in the aggrecan response was observed, whereas with inhibition of contractility via Bleb a significant but reduced aggrecan response was still apparent with dynamic stretch.

Because it had been previously shown that perturbations in contractility (18) and alterations in nuclear structural proteins that mediate nuclear strain transfer (17,19) can alter YAP/TAZ signaling, we next determined the extent to which YAP signaling was altered with tensile loading of aligned

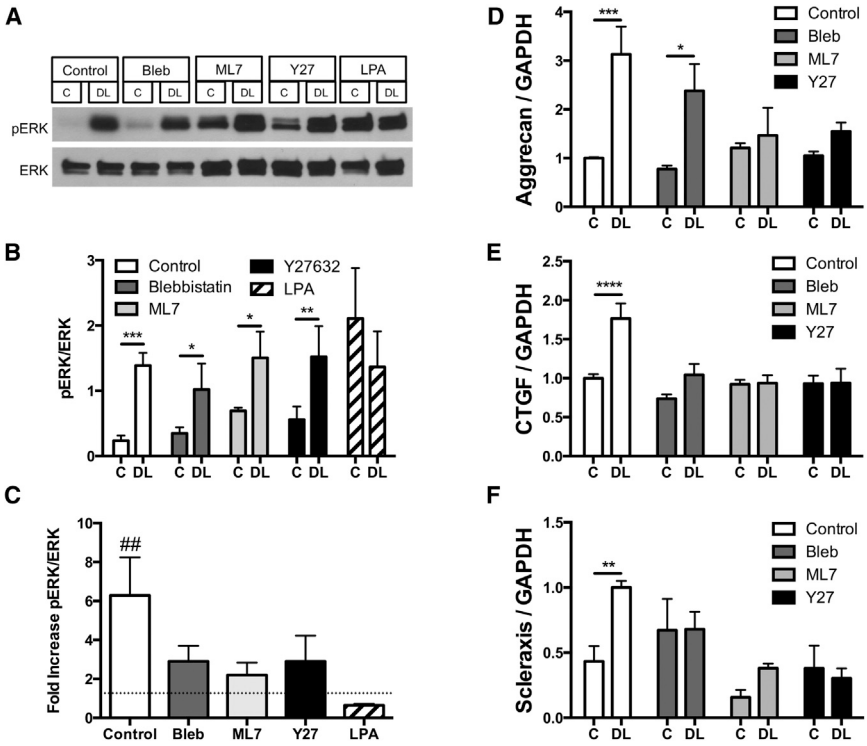

FIGURE 4 Contractility regulates response to dynamic stretch. (*A*) Western blots for phosphorylated ERK1/2 (pERK) and total ERK1/2 (ERK) for MSCs seeded on scaffolds and dynamically loaded (DL) to 3% strain at 1 Hz for 15 min with inhibition or activation of contractility (Bleb, 50 μM, ML7: 25 μM; Y27632, 10 μM; CytoD, 2.5 μM; LPA: 50 μM). Densitometry for (*B*) Western blots (mean $\pm$ SE; $n = 3$/group) plotted as a ratio of pERK/ERK and (*C*) as the fold increase in pERK/ERK with loading. Gene expression measured by (*D*) RT-PCR for the cartilage marker aggrecan, (*E*) the growth factor CTGF, and (*F*) the tendon transcription factor scleraxis. Loading was administered for 6 h per day on two consecutive days; data represent the combined response of four independent experiments. (Mean $\pm$ SE, $n = 9$–12/group, two-way ANOVA with Tukey's post hoc testing.)

scaffolds, and the role of cytoskeletal tension in this process. In unloaded scaffolds, YAP was primarily cytoplasmic, despite the presence of stress fibers (Fig. 5) and the high bulk modulus of both the PCL and the electrospun PCL scaffolds (4). This suggests that the cellular interpretation of the fibrous microenvironment is more akin to that of a soft substrate. Conversely, with 30 or 360 min of dynamic tensile loading, a significant increase in the nuclear/cytoplasmic YAP was observed (Fig. 5, *A* and *B*). Twelve hours after cessation of loading (for the 360-min loading cycle), the nuclear/cytoplasmic YAP returned to baseline levels. With inhibition of ROCK (using Y27632), YAP remained cytoplasmic in free swelling conditions (Fig. 5 *C*) and there was a significant reduction in YAP nuclear localization with 30 min of dynamic stretch (Fig. 5 *D*). Conversely, when cytoskeletal tension was reduced (but nuclear deformation was preserved) by inhibition of MLCK (with ML7), YAP translocation to the nucleus was still observed with 30 min of dynamic stretch (Fig. 5 *D*).

Based on the observation that strain transfer to the nucleus through F-actin was important for the MSC response to dynamic tensile loading, we next assayed the specific role of the connections the nucleus makes to the actin cytoskeleton through nesprin 1 giant. Specifically, we assayed the importance of this structural protein for transfer of strain to the nucleus and the YAP response to dynamic stretch. For these experiments, MSCs were infected with lentiviral vectors containing miRNA directed at the N-terminal region of nesprin 1 giant or a negative control sequence (miRneg) followed by seeding onto aligned scaffolds and application of dynamic stretch for 30 min. Knockdown was verified by dot blot for nesprin 1 after 1-MDa size filtration of whole cell lysate. Analysis of GFP expression via flow cytometry indicated ~70% infection efficiency (not shown), which resulted in ~40% knockdown of nesprin-1 giant compared to cells infected with nontargeting miRNA sequences (Fig. 6 *A*). Expression of nesprin 2 giant (a paralog of nesprin 1 giant) was low in these cells (as indicated by RT-PCR and dot blot), and its expression was not significantly altered by nesprin 1 giant knockdown (not shown). Knockdown of nesprin 1 giant via targeting of the actin binding calponin-homology domain did not alter the basal nuclear aspect ratio but did result in significantly less nuclear deformation at 12 and 15% applied strain (Fig. 6 *B*). This is consistent with previous work using KASH-domain-dominant negative vectors where deformation was applied to the cytoskeleton using a micropipette (34). Next, we assessed the YAP signaling response in the context of dynamic stretch with this perturbation of the LINC complex. YAP staining on aligned scaffolds was evenly distributed throughout the cytoplasm in nonloaded control cells (Fig. 6 *C*). With 30 min of dynamic tensile stretch, YAP localized to the nucleus in control cells (Fig. 6 *C*) but remained in the cytoplasm in nesprin 1 giant knockdown cells. Quantification showed a significant increase in the nuclear/cytoplasmic YAP in control cells with loading that was almost completely abrogated in the context of nesprin 1 giant knockdown (Fig. 6 *D*).

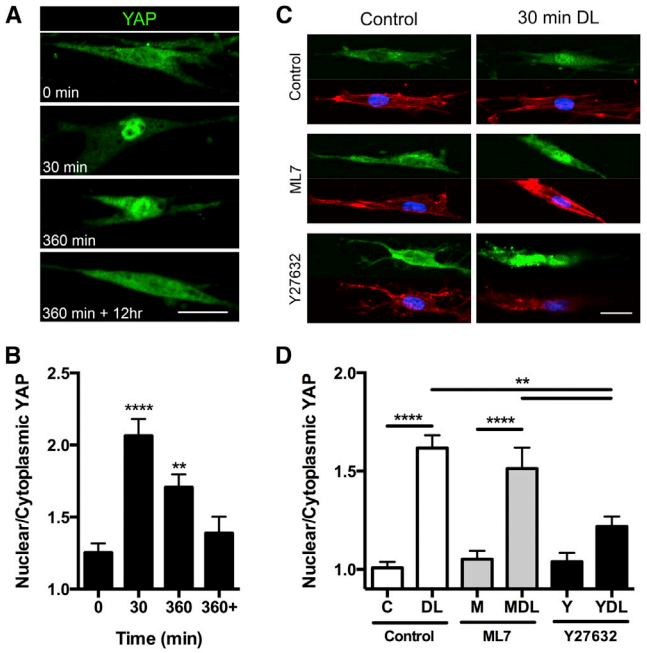

FIGURE 5 YAP signaling is activated by dynamic stretch and requires strain transfer to the nucleus but not cytoskeletal tension. Representative *z*-projected images of (*A*) YAP staining and (*B*) quantification of the nuclear/cytoplasmic YAP for cells seeded on scaffold and dynamically stretched to 3% strain at 1 Hz for 0, 30, or 360 min or 360 min + 12 h of free-swelling culture (scale bar = 25 μm; mean ± SE; n = 38–46 cells/group, two-way ANOVA with Tukey's post hoc testing). Representative *z*-projected images of (*C*) YAP staining (*green*) with associated Actin (*red*) and DAPI (*blue*) with (*D*) quantification after 0 or 30 min of loading under control conditions or with the ROCK inhibitor Y27632 (10 μM) or the MLCK inhibitor ML7 (25 μM). (Mean ± SE, n = 26–34 cells/group, two-way ANOVA with Tukey's post hoc testing; $^{**}p < 0.01$, $^{****}p < 0.0001$.) To see this figure in color, go online.

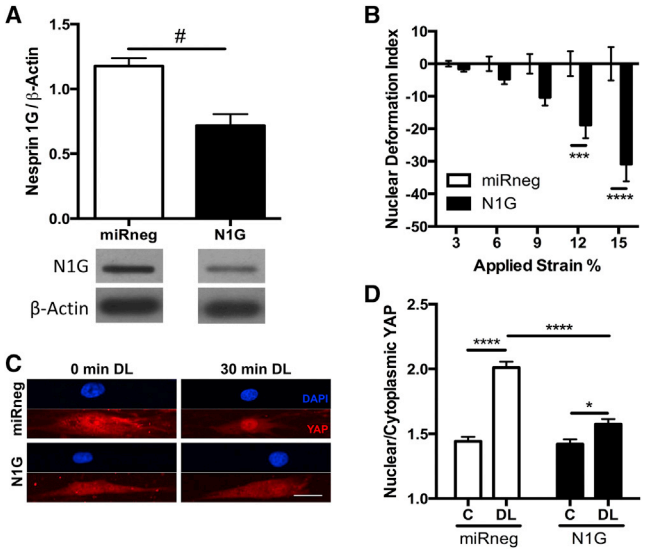

FIGURE 6 YAP signaling requires strain transfer to the nucleus through nesprin-1 giant. (*A*) Knockdown of nesprin-1 giant was performed using lentiviral delivery of miRNA, and knockdown was verified by dot blot for nesprin 1 after 1-MDa size filtration. (*B*) Quantification of the nuclear deformation index with knockdown of nesprin-1 giant compared to control cells (miRneg). Positive index indicates deformations larger than control, negative index indicates deformations less than control (mean ± SE, n = 146–149 cells/group). With less nesprin-1 giant to connect the nucleus to the cytoskeleton, smaller deformations occur. (*C*) Images of YAP (*bottom*) and DAPI (*top*) stained nuclei on aligned scaffolds with or without 30 min of dynamic tensile loading (DL, 3% strain; 1 Hz, scale = 25 μm) and with or without nestrpin-1 giant knockdown. (*D*) Quantification of the nuclear/cytoplasmic YAP for control (noted as "*C*") or dynamically loaded (*DL*) cells. (Mean ± SE, n = 33–41 cells/group; # $p < 0.05$, $^{*}p < 0.05$, $^{***}p < 0.001$, $^{****}p < 0.0001$.) To see this figure in color, go online.

DISCUSSION

Fiber-reinforced soft tissues are exposed to large loads and deformations that are transmitted through their hierarchical extracellular matrix to both cells and their nuclei within (20), regulating numerous cellular processes and playing important roles in the formation, maintenance, and ultimately degeneration of these tissues. In the context of engineered replacements, it will be important to understand both the extent to which these macro-to-microscale deformations are recapitulated in the engineered constructs and the mechanoresponsiveness of the cell types used in the fabrication of these constructs. MSCs are widely used in these types of applications (4), and it is well established that they respond to mechanical signals in a manner that is dependent on a contractile cytoskeleton (1,2). As with native tissue cells, nuclei within MSCs also undergo marked deformations with applied tensile stretch (20,23,24). In this study, we found that the presence of a patent actin cytoskeleton, the tension within this cytoskeletal network, and the connections it makes to the nucleus through nesprin 1 giant, regulate the transmission of strain to the nucleus. We further demonstrated differential short- and long-term response of MSCs to dynamic tensile loading based on the contractility state. Specifically, we showed that while a patent actin cytoskeleton and nuclear connectivity (via the LINC complex) is essential for cytoskeletal strain transfer to the nucleus and activation of the YAP/TAZ pathway with dynamic stretch, other mechanoactive signaling pathways (e.g., ERK signaling) can be activated in the absence of nuclear strain transfer.

Consistent with previous studies using other cell types (31), we found that decreasing contractility reduces actomyosin forces that prestress the MSC nucleus, resulting in an increase in nuclear height and a decrease in projected nuclear area. This prestress dictates the extent to which additional deformation can be transferred to the nucleus. Loss of both contractility and stress fibers, by ROCK inhibition or actin depolymerization, resulted in a significant decrease in nuclear strain transfer, likely due to a loss of the cytoskeletal-to-nucleoskeletal connectivity required for transmission. Our observation of a loss of stress fibers with ROCK inhibition is consistent with previous work, which showed that ROCK directly regulates actin polymerization and depolymerization through the LIM-kinase and cofilin

pathway (35). Interestingly, treatment with ML7 resulted in a loss of contractility, but maintenance of actin stress fibers. Under this scenario, we observed a decrease in the prestress acting on the nucleus (i.e., a smaller nuclear projected area), but an increase in nuclear deformation with applied stretch. This suggested that the remaining stress fibers were capable of transferring strain to the nucleus. Conversely, when contractility was increased (via the addition of LPA), the higher forces acting on the nucleus resulted in compression in the z axis, flattening and stabilizing the nucleus, thus preventing additional strain from being transmitted to this organelle. This increased prestrain in the baseline state may also result in stiffening of the nucleus, due to its hyperelastic strain stiffening characteristics (36).

In addition to nuclear strain transfer, the mechanoresponsivity of cells was differentially influenced by a change in contractility. Independent of nuclear deformation, a decrease in cytoskeletal tension resulted in a small decrease in activation of the ERK1/2 pathway and significant decrease in scleraxis gene expression in response to mechanical loading. This may be due, at least in part, to the fact that many mechanosensitive proteins within focal adhesions, which are known to activate ERK, depend on forced unfolding events. For these mechanosensory events localized to the cell membrane, the amount of strain transfer to the nucleus is likely less important than the concentration of stress in the membrane. One would predict that any decrease in cytoskeletal tension would result in lower stresses within the cell, particularly at actin-associated mechanosensory complexes such as focal adhesions (9,37) and the LINC complex (17,38).

Of note, however, not all mechanically regulated genes were equally affected by a decrease in contractility. Some genes, for instance aggrecan, were less sensitive to a loss in contractility. This may be due to the fact that aggrecan expression is enhanced with inhibition of contractility (39). Additionally, the ERK response to applied load was not prevented when cytoskeletal tension was reduced using any of the inhibitors. This may be due to the fact that other mechanosensitive pathways can activate ERK (such as stretch-activated ion channels) that are less sensitive to a loss in cytoskeletal tension, depending instead on membrane tension (40,41). These channels are mechanosensitive even in artificial bilayers that lack cytoskeletal components (42), where they increase their opening probability in proportion to the level of tension applied to the membrane.

Unlike these early signaling events, the response of the YAP signaling pathway required stress fibers and cytoskeletal strain transfer to the nucleus. Both of these were lost with ROCK inhibition but maintained with MLCK inhibition. This would point to a cytoskeletal and Rho-GTPase-dependent mechanotransduction mechanism, whereby strain transfer into the cell through a patent actin cytoskeleton to the nucleus is necessary for the YAP signaling in response to dynamic tensile loading. However, with longer-term inhibition of cytoskeletal tension during loading, the induction of CTGF, a downstream gene activated by YAP/TAZ, was reduced. This is likely due to longer-term loss of cytoskeletal tension feeding back to reduce stress fibers and cytoskeletal strain transfer.

Further supporting the observation that a loss of stress fibers decreases nuclear strain transfer, knockdown of the LINC complex component nesprin-1 giant attenuated nuclear deformation with stretch. Also consistent with these observations, loss of the cytoskeletal to nuclear connectivity through knockdown of nesprin-1 giant reduced the YAP response to dynamic stretch. While the specific cytoskeletal or nucleoskeletal molecule responsible for YAP mechanical activation is unclear, these data suggest that cytoskeletal forces exerted on the nucleus can regulate its activation. What is clear is that the mechanosensory portion of the YAP/TAZ pathway actually functions through a noncanonical (i.e., LATS-independent) mechanism (18). Given that normal YAP nuclear localization has been shown to occur on poly-L-lysine coated substrates, this unknown regulator is likely not a component of integrin-based focal adhesions (43). Instead, forces in the cytoskeleton itself, or the connections it forms with the nucleus, may regulate this molecule. It has been proposed that LATS-independent YAP signaling in response to mechanical factors likely requires an unknown serine kinase, which is regulated by force in the cytoskeleton (44). Given that knockdown of nesprin 1 giant decreases nuclear deformation but does not decrease cell contractility (31), the data presented here suggests that transmission of force through the cytoskeleton and to the LINC complex is important for regulation of this kinase.

In summary, our results suggest that the MSC nucleus is under a state of prestress and strain that is dictated by the level of actomyosin contractility within the cell, and that this prestrain regulates the deformability of the nucleus when exogenous stretch is applied to the cell. This then mediates response to physical signals transmitted to the cell from the microenvironment. A nucleus with high prestress has low deformability while a nucleus with low prestress has high deformability, as long as the connecting actin stress fibers are intact. A loss of tension in the prestressed cytoskeletal network reduces, but does not prevent, activation of the YAP and ERK signaling pathways in response to applied dynamic stretch. However, complete loss of either a patent actin cytoskeleton or the connections mediated by the LINC complex (and the strain transfer to the nucleus that both enable) inhibits YAP signaling in response to stretch. Thus, if both membrane and cytoskeletal-to-nuclear mechanotransduction pathways exist (Fig. 7 *A*), loss of strain transfer would prevent the activation of cytoskeletal- and nuclear-associated mechanosensitive elements (Fig. 7 *B*). In contrast, when only cytoskeletal tension is reduced, a lower nuclear prestrain allows for larger nuclear deformations, and the cytoskeletal mechanotransduction is maintained. These results support the idea that

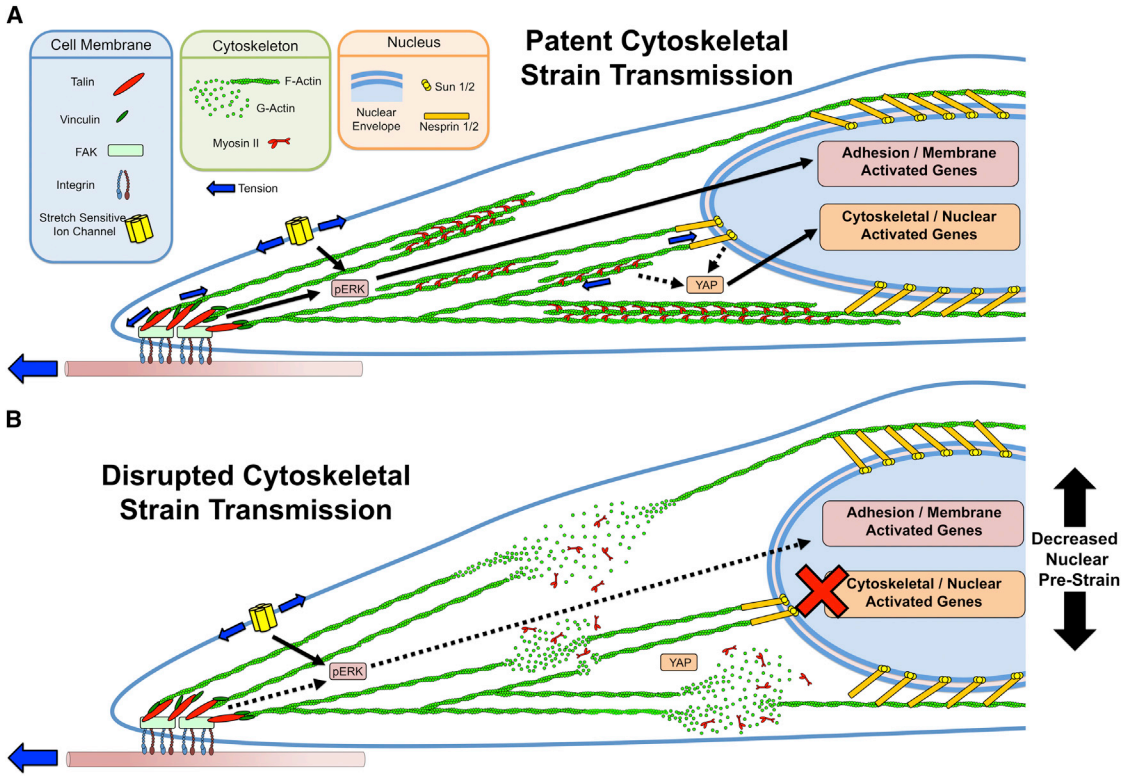

FIGURE 7 Schematic illustration of the differing routes of mechanotransduction. Mechanoactivation may occur via cell membrane-mediated mechanotransduction modules or through cytoskeletal/nuclear strain transfer-mediated mechanotransduction modules. (*A*) In baseline conditions, both pathways are likely operative. (*B*) When ROCK is inhibited with Y27632, a decrease in nuclear prestrain and depolymerization of actin is observed; when nesprin-1 giant levels are reduced, cytoskeletal strain transfer to the nucleus is likewise compromised. This leads to a loss in the cytoskeletal-to-nuclear strain transfer necessary for YAP activation, but does not completely abrogate signals originating as a result of tension at the cell membrane. To see this figure in color, go online.

cytoskeletal strain transfer into the cell is important for YAP mechanosensing events. Despite this, the specific stretch-sensitive molecules responsible for the mechanomodulation of YAP signaling through noncanonical pathways remain unclear (44). Given that both focal adhesion and LINC complexes provide the termini for the actin cytoskeleton, understanding how force is transmitted through these complexes to activate proteins within will be important for elucidating the molecular mechanisms by which contractility regulates the stem cell response to tensile stretch and ultimately lineage specification in mechanically loaded environments.

SUPPORTING MATERIAL

One figure is available at http://www.biophysj.org/biophysj/supplemental/S0006-3495(15)00495-6.

AUTHOR CONTRIBUTIONS

T.P.D. and R.L.M. designed the experiments; T.P.D., B.D.C., Z.E.S., and S.-J.H. performed the experiments; T.P.D. and Z.E.S. built the tensile device; T.P.D. and B.D.C. analyzed the data; and T.P.D. and R.L.M. wrote the article.

ACKNOWLEDGMENTS

The authors gratefully acknowledge Ms. Claire McLeod for helpful discussions and MATLAB coding for edge-detection algorithms. The authors also gratefully acknowledge the use of the confocal imaging resources of the Philadelphia VA Medical Center.

This work was supported by the National Institutes of Health (grants No. R01 EB02425 and No. R01 AR056624). Additional support was provided from a University of Pennsylvania University Research Foundation Award, the Montague Research Award at the Perelman School of Medicine, a grant from the Penn Center for Musculoskeletal Disorders (No. P30 AR050950), and a training grant from the National Institutes of Health (No. T32 AR007132).

REFERENCES

1. Engler, A. J., S. Sen, …, D. E. Discher. 2006. Matrix elasticity directs stem cell lineage specification. *Cell.* 126:677–689.
2. McBeath, R., D. M. Pirone, …, C. S. Chen. 2004. Cell shape, cytoskeletal tension, and RhoA regulate stem cell lineage commitment. *Dev. Cell.* 6:483–495.
3. Angele, P., D. Schumann, …, R. Kujat. 2004. Cyclic, mechanical compression enhances chondrogenesis of mesenchymal progenitor cells in tissue engineering scaffolds. *Biorheology.* 41:335–346.
4. Baker, B. M., R. P. Shah, …, R. L. Mauck. 2011. Dynamic tensile loading improves the functional properties of mesenchymal stem

cell-laden nanofiber-based fibrocartilage. *Tissue Eng. Part A.* 17:1445–1455.

5. Fu, J., Y. K. Wang, …, C. S. Chen. 2010. Mechanical regulation of cell function with geometrically modulated elastomeric substrates. *Nat. Methods.* 7:733–736.
6. Bershadsky, A. D., N. Q. Balaban, and B. Geiger. 2003. Adhesion-dependent cell mechanosensitivity. *Annu. Rev. Cell Dev. Biol.* 19:677–695.
7. Volkers, L., Y. Mechioukhi, and B. Coste. 2014. Piezo channels: from structure to function. *Pflugers Arch.* 467:95–99.
8. Dumbauld, D. W., K. E. Michael, …, A. J. Garcia. 2010. Focal adhesion kinase-dependent regulation of adhesive forces involves vinculin recruitment to focal adhesions. *Biol. Cell.* 102:203–213.
9. Pasapera, A. M., I. C. Schneider, …, C. M. Waterman. 2010. Myosin II activity regulates vinculin recruitment to focal adhesions through FAK-mediated paxillin phosphorylation. *J. Cell Biol.* 188:877–890.
10. Margadant, F., L. L. Chew, …, M. Sheetz. 2011. Mechanotransduction in vivo by repeated talin stretch-relaxation events depends upon vinculin. *PLoS Biol.* 9:e1001223.
11. Grashoff, C., B. D. Hoffman, …, M. A. Schwartz. 2010. Measuring mechanical tension across vinculin reveals regulation of focal adhesion dynamics. *Nature.* 466:263–266.
12. Carisey, A., R. Tsang, …, C. Ballestrem. 2013. Vinculin regulates the recruitment and release of core focal adhesion proteins in a force-dependent manner. *Curr. Biol.* 23:271–281.
13. Papagrigoriou, E., A. R. Gingras, …, J. Emsley. 2004. Activation of a vinculin-binding site in the talin rod involves rearrangement of a five-helix bundle. *EMBO J.* 23:2942–2951.
14. del Rio, A., R. Perez-Jimenez, …, M. P. Sheetz. 2009. Stretching single talin rod molecules activates vinculin binding. *Science.* 323:638–641.
15. Pajerowski, J. D., K. N. Dahl, …, D. E. Discher. 2007. Physical plasticity of the nucleus in stem cell differentiation. *Proc. Natl. Acad. Sci. USA.* 104:15619–15624.
16. Na, S., O. Collin, …, N. Wang. 2008. Rapid signal transduction in living cells is a unique feature of mechanotransduction. *Proc. Natl. Acad. Sci. USA.* 105:6626–6631.
17. Guilluy, C., L. D. Osborne, …, K. Burridge. 2014. Isolated nuclei adapt to force and reveal a mechanotransduction pathway in the nucleus. *Nat. Cell Biol.* 16:376–381.
18. Dupont, S., L. Morsut, …, S. Piccolo. 2011. Role of YAP/TAZ in mechanotransduction. *Nature.* 474:179–183.
19. Bertrand, A. T., S. Ziaei, …, C. Coirault. 2014. Cellular microenvironments reveal defective mechanosensing responses and elevated YAP signaling in LMNA-mutated muscle precursors. *J. Cell Sci.* 127:2873–2884.
20. Han, W. M., S. J. Heo, …, D. M. Elliott. 2013. Macro- to microscale strain transfer in fibrous tissues is heterogeneous and tissue-specific. *Biophys. J.* 105:807–817.
21. Upton, M. L., C. L. Gilchrist, …, L. A. Setton. 2008. Transfer of macroscale tissue strain to microscale cell regions in the deformed meniscus. *Biophys. J.* 95:2116–2124.
22. Bruehlmann, S. B., P. A. Hulme, and N. A. Duncan. 2004. In situ intercellular mechanics of the bovine outer annulus fibrosus subjected to biaxial strains. *J. Biomech.* 37:223–231.
23. Nathan, A. S., B. M. Baker, …, R. L. Mauck. 2011. Mechano-topographic modulation of stem cell nuclear shape on nanofibrous scaffolds. *Acta Biomater.* 7:57–66.
24. Heo, S. J., N. L. Nerurkar, …, R. L. Mauck. 2011. Fiber stretch and reorientation modulates mesenchymal stem cell morphology and fibrous gene expression on oriented nanofibrous microenvironments. *Ann. Biomed. Eng.* 39:2780–2790.
25. Nerurkar, N. L., B. M. Baker, …, R. L. Mauck. 2009. Nanofibrous biologic laminates replicate the form and function of the annulus fibrosus. *Nat. Mater.* 8:986–992.
26. Huang, A. H., M. J. Farrell, …, R. L. Mauck. 2010. Long-term dynamic loading improves the mechanical properties of chondrogenic mesenchymal stem cell-laden hydrogel. *Eur. Cell. Mater.* 19:72–85.
27. Baker, B. M., A. S. Nathan, …, R. L. Mauck. 2010. The influence of an aligned nanofibrous topography on human mesenchymal stem cell fibrochondrogenesis. *Biomaterials.* 31:6190–6200.
28. Aratyn-Schaus, Y., P. W. Oakes, …, M. L. Gardel. 2010. Preparation of complaint matrices for quantifying cellular contraction. *J. Vis. Exp.* 46:2173. http://dx.doi.org/10.3791/2173.
29. Tseng, Q., E. Duchemin-Pelletier, …, M. Théry. 2012. Spatial organization of the extracellular matrix regulates cell-cell junction positioning. *Proc. Natl. Acad. Sci. USA.* 109:1506–1511.
30. Dembo, M., and Y. L. Wang. 1999. Stresses at the cell-to-substrate interface during locomotion of fibroblasts. *Biophys. J.* 76:2307–2316.
31. Chancellor, T. J., J. Lee, …, T. Lele. 2010. Actomyosin tension exerted on the nucleus through nesprin-1 connections influences endothelial cell adhesion, migration, and cyclic strain-induced reorientation. *Biophys. J.* 99:115–123.
32. Khatau, S. B., C. M. Hale, …, D. Wirtz. 2009. A perinuclear actin cap regulates nuclear shape. *Proc. Natl. Acad. Sci. USA.* 106:19017–19022.
33. Ramdas, N. M., and G. V. Shivashankar. 2014. Cytoskeletal control of nuclear morphology and chromatin organization. *J. Mol. Biol.* 427:695–706.
34. Lombardi, M. L., D. E. Jaalouk, …, J. Lammerding. 2011. The interaction between nesprins and sun proteins at the nuclear envelope is critical for force transmission between the nucleus and cytoskeleton. *J. Biol. Chem.* 286:26743–26753.
35. Maekawa, M., T. Ishizaki, …, S. Narumiya. 1999. Signaling from Rho to the actin cytoskeleton through protein kinases ROCK and LIM-kinase. *Science.* 285:895–898.
36. Caille, N., O. Thoumine, …, J. J. Meister. 2002. Contribution of the nucleus to the mechanical properties of endothelial cells. *J. Biomech.* 35:177–187.
37. Dumbauld, D. W., H. Shin, …, A. J. García. 2010. Contractility modulates cell adhesion strengthening through focal adhesion kinase and assembly of vinculin-containing focal adhesions. *J. Cell. Physiol.* 223:746–756.
38. Luxton, G. W., E. R. Gomes, …, G. G. Gundersen. 2010. Linear arrays of nuclear envelope proteins harness retrograde actin flow for nuclear movement. *Science.* 329:956–959.
39. Woods, A., and F. Beier. 2006. RhoA/ROCK signaling regulates chondrogenesis in a context-dependent manner. *J. Biol. Chem.* 281:13134–13140.
40. Anishkin, A., S. H. Loukin, …, C. Kung. 2014. Feeling the hidden mechanical forces in lipid bilayer is an original sense. *Proc. Natl. Acad. Sci. USA.* 111:7898–7905.
41. Schmidt, D., J. del Mármol, and R. MacKinnon. 2012. Mechanistic basis for low threshold mechanosensitivity in voltage-dependent K^+ channels. *Proc. Natl. Acad. Sci. USA.* 109:10352–10357.
42. Brohawn, S. G., Z. Su, and R. MacKinnon. 2014. Mechanosensitivity is mediated directly by the lipid membrane in TRAAK and TREK1 K^+ channels. *Proc. Natl. Acad. Sci. USA.* 111:3614–3619.
43. Zhao, B., L. Li, …, K. L. Guan. 2012. Cell detachment activates the Hippo pathway via cytoskeleton reorganization to induce anoikis. *Genes Dev.* 26:54–68.
44. Low, B. C., C. Q. Pan, …, M. Sheetz. 2014. YAP/TAZ as mechanosensors and mechanotransducers in regulating organ size and tumor growth. *FEBS Lett.* 588:2663–2670.

Biophysical Journal

Supporting Material

Cytoskeletal to Nuclear Strain Transfer Regulates YAP Signaling in Mesenchymal Stem Cells

Tristan P. Driscoll,[1,2] Brian D. Cosgrove,[1,2] Su-Jin Heo,[1,2] Zach E. Shurden,[1,2] and Robert L. Mauck[1,2,3,4,*]

[1]McKay Orthopaedic Research Laboratory, Department of Orthopaedic Surgery, Perelman School of Medicine, [2]Department of Bioengineering, School of Engineering and Applied Science, and [3]Department of Mechanical Engineering and Applied Mechanics, School of Engineering and Applied Science, University of Pennsylvania, Philadelphia, Pennsylvania; and [4]Translational Musculoskeletal Research Center, Philadelphia VA Medical Center, Philadelphia, Pennsylvania

Supplemental Figures

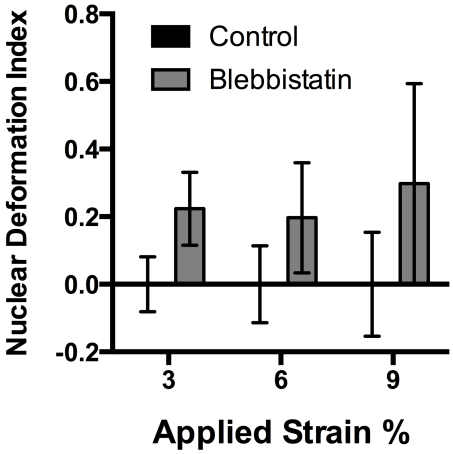

Supplemental Figure 1: Nuclear deformation index for MSCS treated with the myosin inhibitor Blebbistatin. Mean +/- SEM, n>30 cells / group.